Applied Surface Science 476 (2019) 533–538

Contents lists available at ScienceDirect

Applied Surface Science

journal homepage: www.elsevier.com/locate/apsusc

Full Length Article

The role of edge-oxidized graphene to improve the thermopower of p-type bismuth telluride-based thick films

Young Min Cho[a,b,1], Kyung Tae Kim[a,*,1], Gi Seung Lee[a], Soo Hyung Kim[b]

[a] Metal Powder Department, Korea Institute of Materials Science, 797 Changwon-daero, Changwon-si, Gyeongnam 51508, Republic of Korea
[b] Department of Nanoenergy Engineering, Pusan National University, 1268-50 Samnangjin-ro, Miryang-si, Gyeongnam 50463, Republic of Korea

ARTICLE INFO

Keywords:
Edge-oxidized graphene
Bismuth telluride
Thick film
Thermopower

ABSTRACT

Edge-oxidized graphene-dispersed $Bi_{0.4}Sb_{1.6}Te_3$ (EOG/BST) thick films are fabricated by the hand-printing of EOG/BST paste followed by a heat-treatment process. Fabricated EOG/BST thick films are approximately 200 μm thick, and the EOGs in the film are dispersed rather than agglomerated but also appear to connect the separated BST grains. A 2 wt% EOG/BST thick film shows a maximum thermopower of 0.00206 W/mK^2, which is approximately 1.7 times higher than the output of 0.00133 W/mK^2 of BST film without EOG. The improved thermopower stems from the EOG, which provides rapid carrier-transport and an increase in the electrical conductivity of the BST film. It has been found that the edge-surface of EOG is chemically bonded with Bi, Te and Sb via interfacial oxygen atoms and the perfect graphite (sp^2) structure of the EOG facilitates rapid movement of the carriers. The carrier mobility of 2 wt% EOG/BST film sample was improved by about 1.75 times without sacrificing the carrier density compared to that of BST film. These results indicate a promising means of using EOG to enhance the electrical properties of thermoelectric thick films, which can be utilized in active coolers and in wearable power generators.

1. Introduction

Energy devices utilizing thermoelectric (TE) effects are considered by many to be promising tools with which to recover wasted heat and for precise temperature control given the reversible conversion between thermal differences these devices offer and the fact that the electrical energy they use is in a solid state [1]. The energy conversion performance capabilities of TE materials can be determined by the dimensionless figure of merit, ZT ($=\alpha^2\sigma T/\kappa$), where σ is the electrical conductivity, α is the Seebeck coefficient, $\alpha^2\sigma$ represents the thermopower, κ is the thermal conductivity and T is the absolute temperature [2,3].

Bismuth telluride based alloys are well known materials for use in practical applications due to their good ZT performance in the temperature range of ambient temperature to 473 K when using various types of TE modules, which are classified by their thicknesses, i.e., either the bulk, thick-film or thin-film types. Given that the thickness of the TE module directly improves the performance depending on the maintenance of the temperature gradient (ΔT), designing and fabricating TE materials with suitable thicknesses is important. That is, although thin-film TE modules (tens of μm) appear to be useful in various applications due to their size, thin TE elements are limited with regard to maintaining a consistent ΔT value compared bulk elements with thicknesses on the mm scale. Thus, recently, many researchers have focused on the thick film types of TE modules with thicknesses in the range of 100–500 μm for self-power generation or for application to CPU coolers in mobile devices [4–6].

However, thick-film TE modules with performance capabilities comparable to those of the bulk have rarely been developed given the difficulty encountered when attempting to create sound thick-film materials. The main reason for this originates from the paste-based fabrication process of thick film. It is known that a large amount of porosity arises with the imperfect densification of printed film using a binder which evaporates after the heat treatment [7]. Furthermore, organic binders are non-conductive and serve to mainly degrade the electrical properties in the film despite the importance of electrical conductivity [8].

To make a conductive TE paste, the first requirement is to resolve the aforementioned problems. However, most research on the fabrication of TE films focus on improvements via a post-treatment and changes of microstructures related to the paste process. For example, Cho et al. introduced TE film fabricated by screen printing with a post-

* Corresponding author.
E-mail address: ktkim@kims.re.kr (K.T. Kim).
[1] Y.M. Cho and K.T. Kim contributed equally to this work as first author.

https://doi.org/10.1016/j.apsusc.2019.01.026
Received 4 September 2018; Received in revised form 30 December 2018; Accepted 3 January 2019
Available online 04 January 2019
0169-4332/

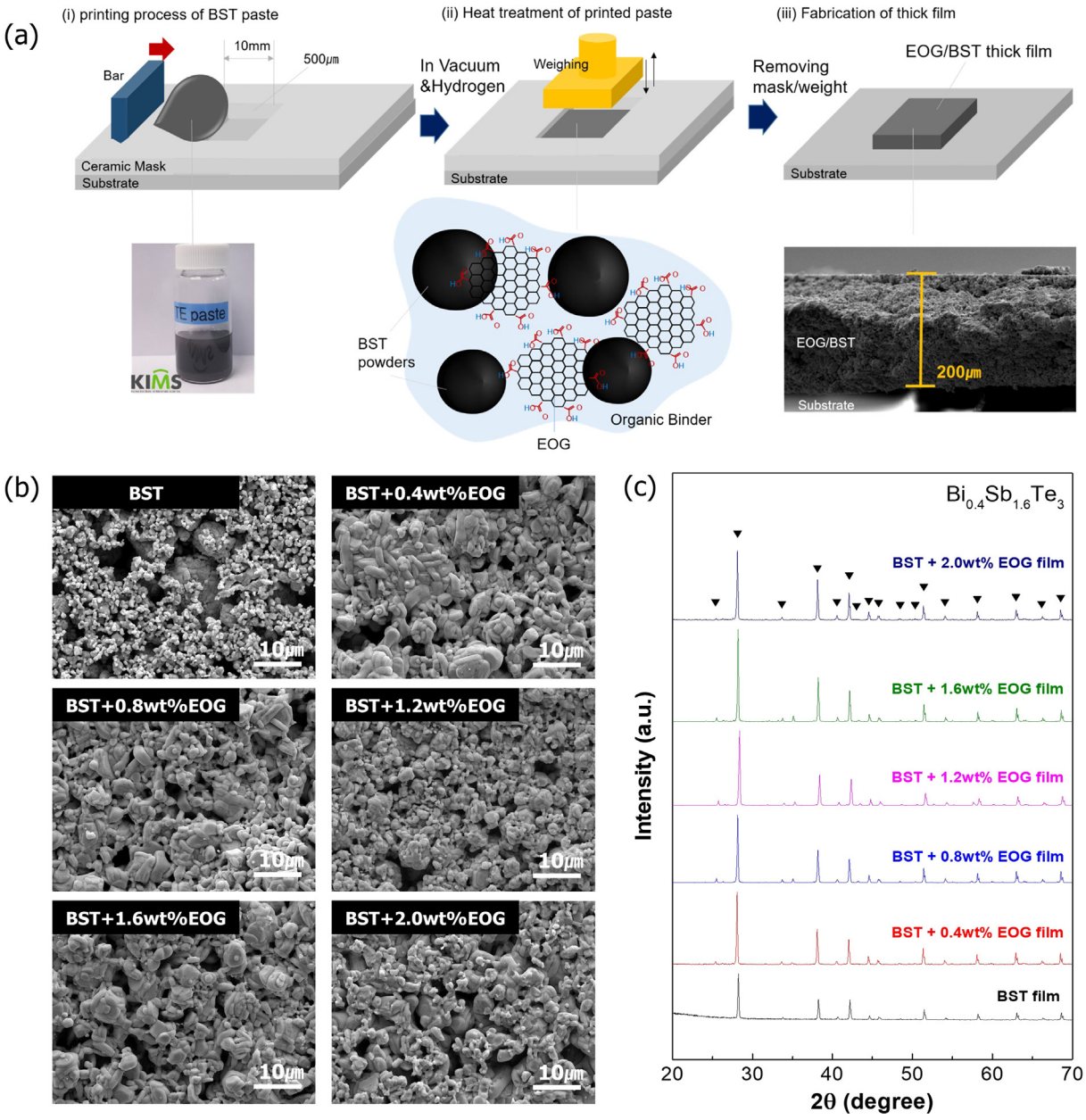

Fig. 1. (a) Schematic illustrations of the fabrication process of EOG/BST thick film using a paste printing process, (b) surface morphologies and (c) XRD patterns of all of the thick films fabricated here.

ionized defect-engineering process [9]. Son et al. reported that Sb_2Te_3 chalcogenidometalate acts as a sintering aid to increase the density during sintering [10]. Thus, conductive TE materials for thick films should be developed to enhance the thermopower ($\alpha^2\sigma$), which is a representative property related to the power generation capability of these modules.

Here, we introduce edge-oxidized graphene (EOG) to achieve high electrical conductivity in thick film based on p-type bismuth telluride. EOG is a two-dimensional material with relatively complete sp^2 bonds that brings about higher electrical conductivity by twofold than general reduced graphene oxide [11]. In addition, improved electrical properties, especially with regard to thermopower levels, of thermoelectric film can be anticipated when the EOGs are dispersed because the functional group attached at the edge of the graphene allows suitable dispersibility or chemical bonding with the p-type $(Bi,Sb)_2Te_3$ grains.

2. Experimental procedure

Raw materials of bismuth, antimony and tellurium (Materion Co. Ltd, USA) were alloyed into $Bi_{0.4}Sb_{1.6}Te_3$ (BST) powders by a high-energy ball milling process (Fritsch Monomill, Pulverisette, Germany) under 450 rpm for 11 hr. The BST powder was mixed into the paste using an organic binder consisting of 1 wt% ethyl cellulose and α-terpineol (Sigma Aldrich, USA). The EOG was then solutionized in distilled water and was added to BST paste samples at five different contents of 0.4, 0.8, 1.2, 1.6 and 2.0 wt%. The EOG-dispersed BST (EOG/BST) paste was then used to produce a film with a thickness of about 200 μm on an alumina substrate through a hand-printing method, and a two-step heat treatment was carried out to remove organic binders and to sinter the films. The phases of the films were characterized by X-ray diffraction (Rigaku, D/MAX 2500, Japan). The surface morphology of the powders and films were analyzed by field emission scanning electron microscopy (FE-SEM, MIRA3 LM, TESCAN, Czech Republic). To evaluate the

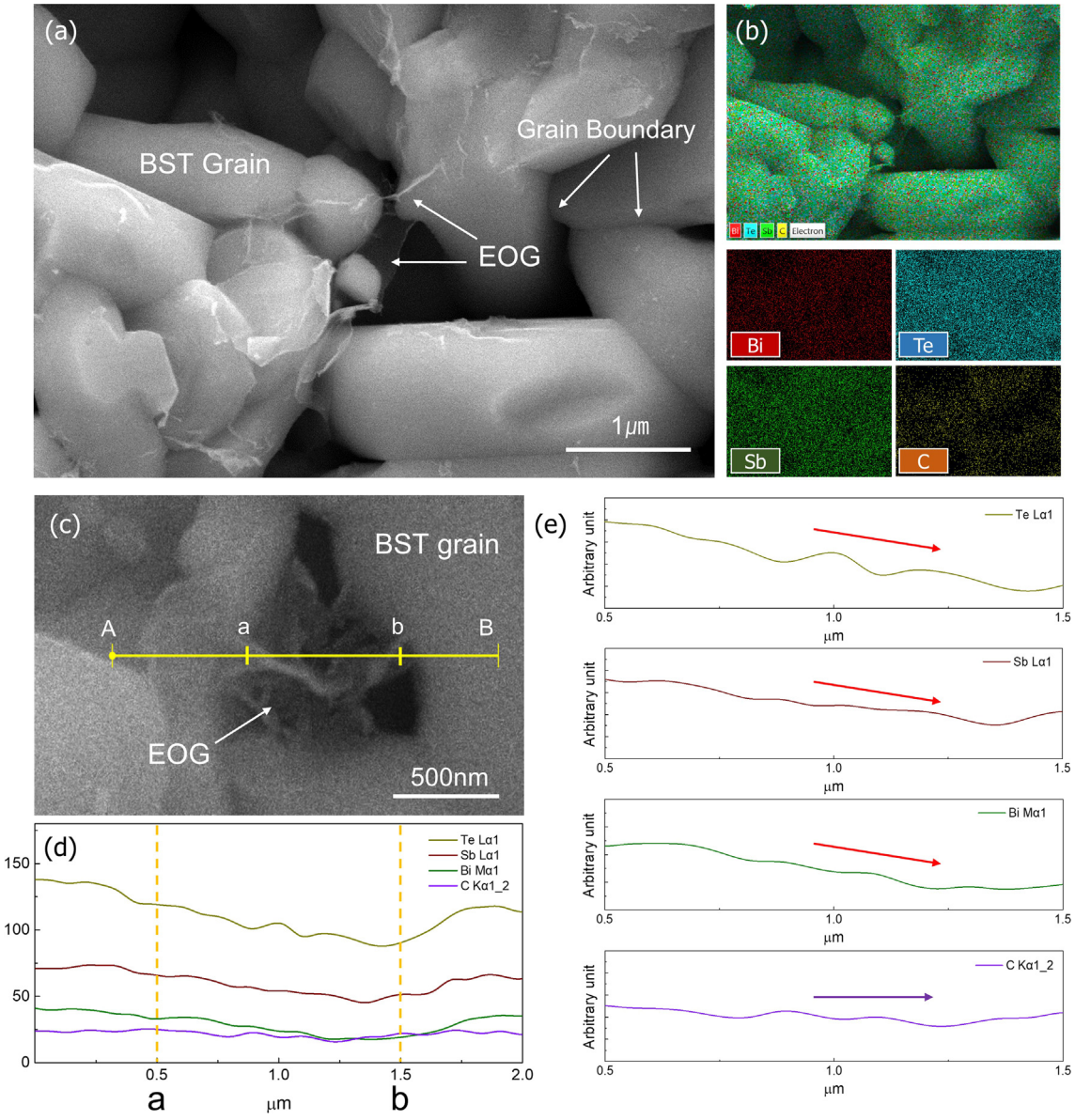

Fig. 2. (a) Enlarged surface image of EOG/BST thick film showing EOG dispersed among BST grains, (b) area EDS results of the image in (a), (c) a SEM image exhibiting EOG present between BST grains, (d) line EDS results on the A-B line and, (e) EDS results on the a-b line for the Bi, Sb, Te and C atoms.

electrical properties of the fabricated TE films, a Hall measurement system (Ecopia, Model AHT55T3, South Korea) and a Seebeck coefficient measurement system were utilized. The bonding between the EOG and the BST matrix was characterized by XPS analysis (AXIS-SUPRA, Kratos, UK).

3. Results and discussion

Fig. 1(a) presents schematic illustrations of the fabrication process of an EOG/BST thick film sample, showing the confirmed thickness of approximately 200 μm. Fig. 1(b) shows the in-plane surface morphologies of fabricated BST/EOG films with different contents of EOG. For comparison, a BST film sample without EOG was fabricated by the same process. In all of the films, most of the BST powders were connected to each other while also being sintered by the heat treatment, although a perfectly smooth surface was not revealed. Fig. 1(c) shows XRD patterns of the fabricated films. This analysis indicates that the phases of all fabricated BST films are in good agreement with JCPDS card No. 72-1836, which corresponds to $Bi_{0.4}Sb_{1.6}Te_3$. However, peaks for graphitic structures were not observed due to the small amount of EOG in all of the films. This implies that the composition of the BST matrix does not change regardless of the addition of EOG and/or the use of a heat treatment.

Fig. 2(a) shows that almost transparent EOG-like film presents on the surface of BST grains which are partly sintered. On the other hand, the location of the EOG-like film provides evidence of the connections among separate BST grain, forming micron-scale empty space caused by the porosity which arises when the organic binder is removed. However, the energy dispersive X-ray spectroscopy (EDS) results shown in Fig. 2(b) indicate unclear differences in the distribution of the carbon atoms. As shown in Fig. 2(c), (d) and (e), the line EDS outcome from EOG-like film on A-B line indicates that carbon is uniformly distributed, whereas only slight distributions of Bi, Sb and Te atoms on a-b line are expected in empty space. Thus, the presence of EOG was confirmed by EDS and the EOGs are continuously connected among the BST grains.

In order to determine how the state of the EOG on the surface of the BST film, the binding energies for each atom in the EOG/BST films were confirmed by an XPS analysis. Fig. 3(a) shows wide-scan results of the

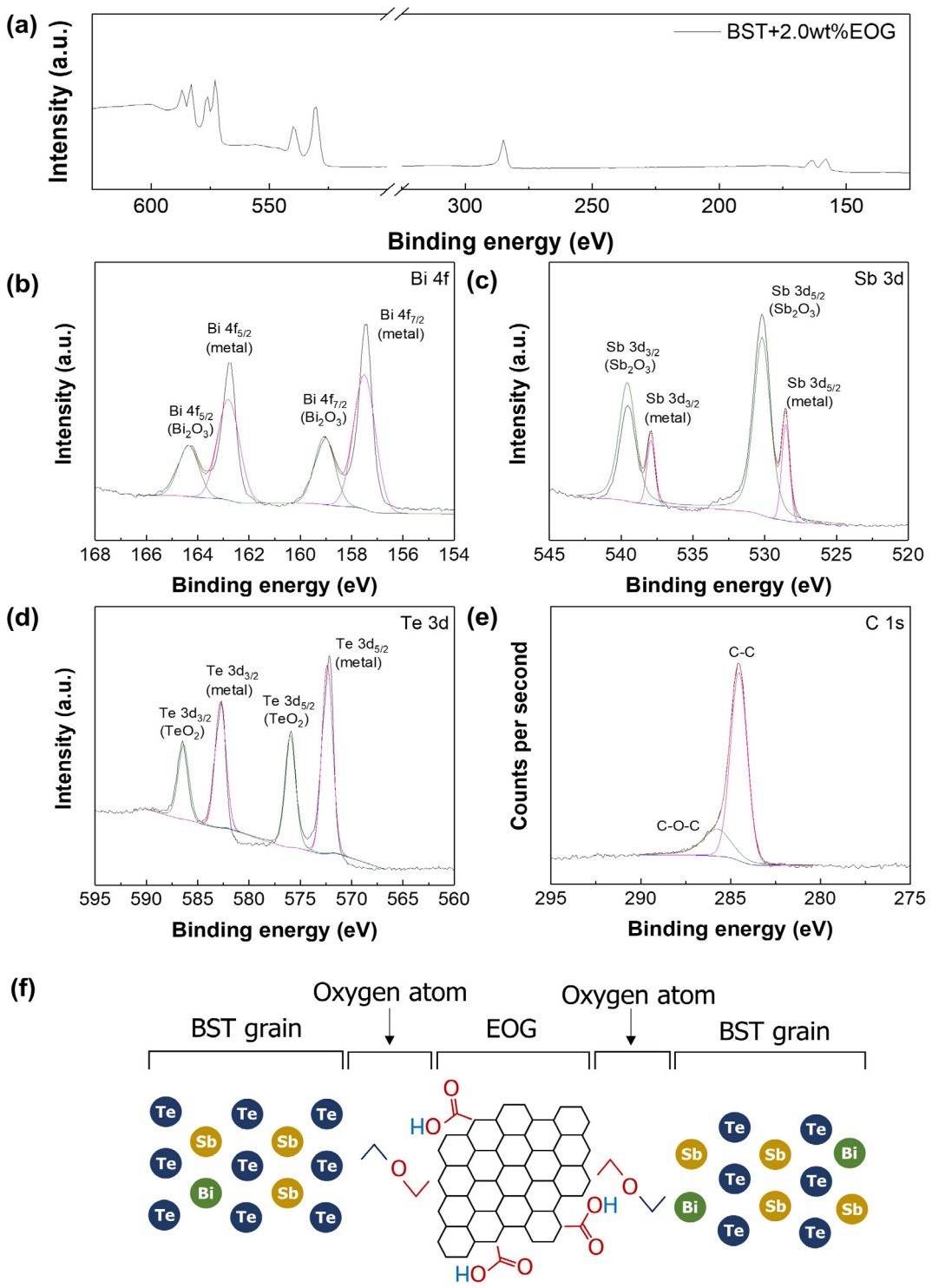

Fig. 3. XPS analysis results of the 2 wt% EOG/BST TE film: (a) wide-scan result of the film; (b–e) narrow-scan result for each instance of the peak deconvolution of the elements and oxidized states for Bi, Sb, Te and C; and (f) a schematic depiction of the interfacial structure between the EOG and the BST grains.

XPS analysis of the surface of the 2.0 wt% EOG/BST film sample. The peaks of Bi, Te, Sb and C in the EOG/BST film are located at around 160, 580, 535 and 285 eV. Fig. 3(b) presents the narrow-scan result of Bi in the 2.0 wt% EOG/BST film. The peaks for Bi $4f_{5/2}$ and Bi $4f_{7/2}$ are located at 162.8 and 157.5 eV, respectively, and two peaks corresponding to the binding energy of Bi_2O_3 at 164.3 and 159.1 eV were revealed without any other peaks representing metallic impurities. As shown in Fig. 3(c) and (d), peaks for not only Sb and Te but also for Sb_2O_3 and TeO_2 which are corresponding oxides of Sb and Te, were identified in the results of the XPS analysis of Bi. Fig. 3(e) presents the narrow-scan results of the XPS analysis of carbon on the surface of the 2.0 wt% EOG-BST film. The C 1s peak and the C-O-C peak were detected at 284.5 and 285.8 eV, respectively, indicating that EOG exists in the film [12]. These results mean that there is a high possibility of oxygen-atom-mediated chemical bonding between the BST and the edges of the EOGs. Given that Bi, Sb and Te are known to have high oxidation behaviors, oxygen-containing functional groups at the side edges of the EOG can act as a feasible medium to form BST oxide at the EOG/BST

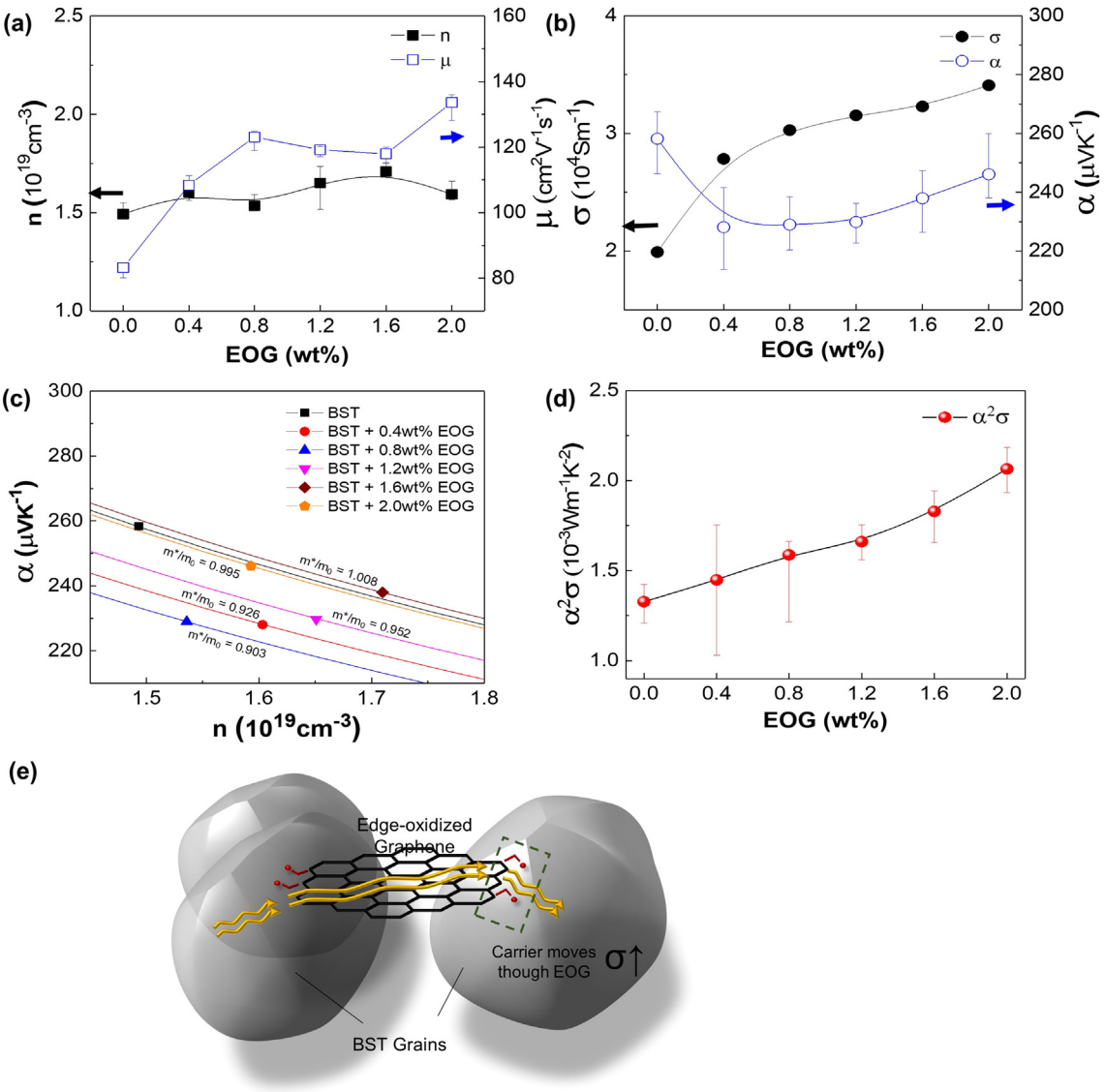

Fig. 4. Variations of (a) the carrier density and mobility, (b) electrical conductivity and Seebeck coefficient as a function of the EOG content, (c) Pisarenko plots showing changes in the Seebeck coefficient with different carrier densities, and (d) power factors with an increase in the EOG contents (e) schematic depiction of BST grains connected by EOG.

interface, as schematically illustrated in Fig. 3(f).

Fig. 4(a) shows the variation of the carrier density (n) and the carrier mobility (μ) in the EOG/BST films as a function of the EOG content. The value of n of approximately $1.5 \times 10^{19}\,cm^{-3}$ of the BST film remains nearly constant regardless of the addition of EOG. Interestingly, the carrier mobility increases with an increase in the EOG content. The carrier mobility of the 2.0 wt% EOG/BST film increased by about 1.6 times, from 83 cm^2/Vs to 133 cm^2/Vs, as compared to that in the BST film without EOG. Fig. 4(b) shows the changes of the electrical conductivity and Seebeck coefficient with the addition of EOG in the BST films at room temperature. Here, σ and α for a thermoelectric material can be expressed using the following equations,

$$\sigma = ne\mu \tag{1}$$

$$\alpha = \frac{8\pi^2 k_B^2}{3eh^2} m^* T \left(\frac{\pi}{3n}\right)^{2/3} \tag{2}$$

where n, μ, k_B, h, and m* are the carrier density, carrier mobility, Boltzmann constant, Planck constant and effective mass, respectively [2]. According to Fig. 4(b), the σ value of the 2 wt% EOG/BST film sample increased to 3.40×10^4 S/m compared to the value of 1.99×10^4 S/m for the BST film without EOG. However, the Seebeck coefficients do not show significant changes, with values in the range of 230–258 μV/K. Fig. 4(c) shows a Pisarenko plot which indicates the relationships between n and α as obtained from all of the samples [13]. According to these relationships, the effective masses of the samples are similar even when EOG is added. That is, these outcomes reveal that EOG does not cause a major enhancement of the Seebeck coefficient in the TE films, though it leads to a major difference in μ to improve the electrical conductivity. In addition, it should be noted that new paths through which carriers move were added to the BST films with the addition of EOG. Therefore, it is necessary to take into account the probability of the following two factors when carriers move between the grains; the grain-grain interface and the grain-EOG interface. Considering the σ and α values, thermopower of 0.00206 W/mK^2 is achieved with the 2 wt% EOG/BST TE film, an increase of 1.6 times with regard to the addition of EOG in the BST TE film, as shown in Fig. 4(d). Furthermore, it can be proven that the increased thermopower is due to accelerated carrier movement through the chemically connected EOG with BST grains, as illustrated in Fig. 4(e).

4. Conclusion

Conductive BST paste using edge-oxidized graphene (EOG) was synthesized and EOG/BST thick films with improved electrical conductivity levels were fabricated. Due to the presence of EOG in the films, it could be confirmed that carriers can pass rapidly along the surface of the complete graphitic structure without stopping, even in porous regions which are not fully densified. In addition, EOGs are physically dispersed but also chemically bonded via interfacial oxygen atoms, stemming from the function groups at the side edges of the EOG. As a result, the mobility and electrical conductivity of the 2 wt% EOG/BST TE films increased by 1.6 times and 1.79 times, respectively, compared to films without EOG. The maximum thermopower reached 0.00206 W/mK^2, which is comparable to that in BST bulk material.

Acknowledgement

We thanks to the support from the Principal R&D project titled as 'Development of Fundamental Technology for Tailoring Materials Properties based on Metastable Microstructure' (Code No. PNK6040) of Korea Institute of Materials Science (KIMS) in Republic of Korea. K.T.K expresses gratitude for a grant (Code no. NRF2016M3A7B4900) from the Core Research Project on Nano-Materials of National Research Foundation (NRF) in Republic of Korea.

References

[1] L.E. Bell, Cooling, heating, generating power, and recovering waste heat with thermoelectric systems, Science 321 (2008) 1457–1461.
[2] G.J. Snyder, E.S. Toberer, Complex thermoelectric materials, Materials For Sustainable Energy: A Collection of Peer-Reviewed Research and Review Articles from Nature Publishing Group, World Scientific, 2011, pp. 101–110.
[3] K.T. Kim, S.Y. Choi, E.H. Shin, K.S. Moon, H.Y. Koo, G.-G. Lee, G.H. Ha, The influence of CNTs on the thermoelectric properties of a CNT/Bi_2Te_3 composite, Carbon 52 (2013) 541–549.
[4] T. Varghese, C. Hollar, J. Richardson, N. Kempf, C. Han, P. Gamarachchi, D. Estrada, R.J. Mehta, Y. Zhang, High-performance and flexible thermoelectric films by screen printing solution-processed nanoplate crystals, Sci. Rep. 6 (2016) 33135.
[5] E. Rogacheva, O. Nashchekina, Y.O. Vekhov, M. Dresselhaus, S. Cronin, Effect of thickness on the thermoelectric properties of PbS thin films, Thin Solid Films 423 (2003) 115–118.
[6] K.T. Kim, T.S. Min, D.W. Kim, Investigation on the thermoelectric properties of bismuth telluride matrix composites by addition of graphene oxide powders, J. Korean Powder Metall. Inst. 23 (2016) 263–269.
[7] M. Mustapha, F. Ismail, O. Mamat, Empirical Relationship between Relative Electrical Conductivity and Relative Density of the Al-Foam Fabricated through Pressure Assisted Sintering/Dissolution Process, IOP Conference Series: Materials Science and Engineering, IOP Publishing, 2011, p. 012014.
[8] N. Kamenka, I. Burgaud, R. Zana, B. Lindman, Electrical conductivity, self-diffusion, and fluorescence probe investigations of the interaction between sodium dodecyl sulfate and ethyl (hydroxyethyl) cellulose, J. Phys. Chem. 98 (1994) 6785–6789.
[9] S.J. Kim, H. Choi, Y. Kim, J.H. We, J.S. Shin, H.E. Lee, M.-W. Oh, K.J. Lee, B.J. Cho, Post ionized defect engineering of the screen-printed $Bi_2Te_{2.7}Se_{0.3}$ thick film for high performance flexible thermoelectric generator, Nano Energy 31 (2017) 258–263.
[10] S.H. Park, S. Jo, B. Kwon, F. Kim, H.W. Ban, J.E. Lee, D.H. Gu, S.H. Lee, Y. Hwang, J.-S. Kim, High-performance shape-engineerable thermoelectric painting, Nat. Commun. 7 (2016) 13403.
[11] J. Park, Y.S. Kim, S.J. Sung, T. Kim, C.R. Park, Highly dispersible edge-selectively oxidized graphene with improved electrical performance, Nanoscale 9 (2017) 1699–1708.
[12] A.K.-V. Alexander V. Naumkin, Stephen W. Gaarenstroom, Cedric J. Powell, NIST Standard Reference Database 20, Version 4.1, in, 2010.
[13] J.P. Heremans, V. Jovovic, E.S. Toberer, A. Saramat, K. Kurosaki, A. Charoenphakdee, S. Yamanaka, G.J. Snyder, Enhancement of thermoelectric efficiency in PbTe by distortion of the electronic density of states, Science 321 (2008) 554–557.